PROCEEDINGS OF SPIE

SPIEDigitalLibrary.org/conference-proceedings-of-spie

Particulate contamination on starshade optical edges

Dylan McKeithen, Stuart Shaklan, Joshua Vawdrey

Dylan McKeithen, Stuart B. Shaklan, Joshua Vawdrey, "Particulate contamination on starshade optical edges," Proc. SPIE 12680, Techniques and Instrumentation for Detection of Exoplanets XI, 1268011 (5 October 2023); doi: 10.1117/12.2677571

SPIE.

Event: SPIE Optical Engineering + Applications, 2023, San Diego, California, United States

Downloaded From: https://www.spiedigitallibrary.org/conference-proceedings-of-spie on 01 Nov 2023 Terms of Use: https://www.spiedigitallibrary.org/terms-of-use

Particulate contamination on starshade optical edges

Dylan McKeithen[a], Stuart B. Shaklan[a], and Joshua Vawdrey[b]

[a]Jet Propulsion Laboratory, California Institute of Technology, Pasadena, California 91109
[b]Brigham Young University, Department of Physics and Astronomy, Provo, Utah 84604

ABSTRACT

The optical edges of a starshade define its outermost perimeter. During astronomical measurements, the edges are exposed to sunlight resulting in glint seen by the telescope. Clean, sharply etched edges are capable of meeting the stringent solar glint scatter requirement. We report on the increased glint that arises from particulate contamination clinging to the edges. We measure the relationship between surface contamination and edge contamination, and compare to a simple edge contaminant population model where the edge acts like a line drawn across the continuous surface. We correlate the level of edge contamination to the degree of increased scatter, and derive an on-orbit contamination requirement that is compatible with the detection of exo-Earths.

Keywords: Starshade, Exoplanets, Habitable Worlds Observatory, High-Contrast Imaging, Particulate Contamination, IEST-STD-CC1246E, Product Cleanliness Level, Percent Area Coverage

1. INTRODUCTION

The discovery and characterization of habitable worlds outside our solar system has been identified as a key priority for the future of space exploration.[1] One of the leading technologies in pursuit of this endeavor is the starshade, a flower-like structure designed to suppress starlight and reveal exoplanets that would otherwise be obscured by stellar glare.[2] The performance of a starshade significantly depends on the condition of its optical edge, the outermost perimeter that defines the apodization function. The edge must have the right outline to control stellar diffraction,[3] and it must be sharp and dark to minimize solar glint.

The quality and cleanliness of this edge play a vital role in the starshade's efficacy. Past work has demonstrated that sharply etched, amorphous metal optical edges have the ability to meet the stringent solar glint scatter requirement.[4] Yet, a significant challenge arises in the form of particulate contamination that can cause additional light scattering. Care must be taken to limit the particulate contamination build up on the starshade to some reasonable level.

While there exist standards, discussed below, to describe the level and nature of particulate contamination on surfaces, there are to our knowledge no corresponding standards for edges. Here, we study the relationship between surface contamination and edge contamination, and develop a model to predict the level of edge contamination given a contaminated surface. We further study the correlation between edge contamination and the increased amount of scattered light, and use this relationship to determine an on-orbit contamination requirement consistent with a maintaining the corresponding solar glint to be fainter than visual magnitude 33 for the HWO starshade concept.

1.1 IEST-STD-CC1246E Surface Contamination Standard

In this research, we utilize the contamination standard set by the Institute of Environmental Sciences and Technology (IEST), IEST-STD-CC1246E.[5] This standard provides comprehensive guidelines for establishing, implementing, and maintaining cleanliness levels for products within cleanrooms and controlled environments. Specifically, the product cleanliness levels (PCLs) defined within the standard denote the level of particulate contamination on sample surfaces. The PCL itself is a metric that refers to the point in the particle distribution where one particle per tenth square meter of this size and greater is found. For example, a surface with a

Further author information: (Send correspondence to Dylan McKeithen)
Dylan McKeithen: E-mail: dylan.m.mckeithen@jpl.nasa.gov, Telephone: +1 (818) 393-3993

Techniques and Instrumentation for Detection of Exoplanets XI, edited by
Garreth J. Ruane, Proc. of SPIE Vol. 12680, 1268011 · © 2023 SPIE
0277-786X · doi: 10.1117/12.2677571

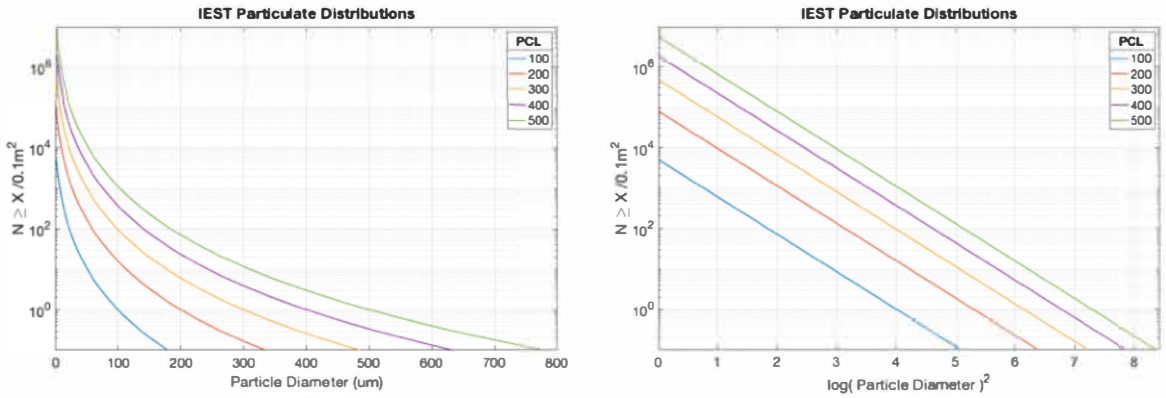
Downloaded From: https://www.spiedigitallibrary.org/conference-proceedings-of-spie on 01 Nov 2023
Terms of Use: https://www.spiedigitallibrary.org/terms-of-use

classification of PCL 500 contains one particle per tenth square meter of size 500 µm or greater. The standard is commonly used throughout the aerospace industry to define requirements on the surface contamination level of parts being manufactured and tested.

According to the standard, particulate contamination has a log-normal distribution of particle sizes, with a geometric mean size of ∼1 µm. These distributions can be represented by a straight line when plotted on a log-log^2 scale. The particle size distribution for 'clean' surfaces can then be expressed as:

$$\log N = -0.926(\log^2(x) - \log^2(\mathrm{PCL})) \tag{1}$$

where N is the number of particles per tenth square meter equal to and greater than the stated size (x), -0.926 is the standardized slope of the line in log-log^2 space, x is the particle size, and PCL is the product cleanliness level.



(a) (b)

Figure 1. (a) IEST Particulate distributions for various PCLs ranging from PCL100 to PCL500 plotted on a log-linear scale. Note that the PCL corresponds to the point in the graph where the distribution crosses 1. (b) Same particulate distributions plotted on a log-log^2 scale, highlighting the linear nature of the distributions on this scale.

Figure 1 demonstrates several distributions generated from eq. 1 ranging from PCL100 to PCL500. Note that when plotted on a log-log^2 scale, the distributions are linear. Further note that the slope of these lines is constant and is standardized to be -0.926. In general, the particulate distributions under study do not conform to this standard slope, and so where relevant, we classify the surface particulate distribution with both a PCL and slope, obtained through a two-parameter least-squares fit of the measured distribution.

In addition to the PCL, it is often useful to classify a contaminated surface with the percent area coverage (PAC), describing the percentage of the surface which is covered by particulates. Generally, the PAC will depend on the shape of the particulates. Assuming circular particles, Ma et. al.,[6] found that the PAC could be estimated as a function of the PCL:

$$\log(\mathrm{PAC}) = -7.245 + 0.926\log^2(\mathrm{PCL}) \tag{2}$$

1.2 Edge Contamination

IEST-STD-CC1246E is the standard descriptor for the characterization of particles present on a surface. Critically, however, there is no analogous standard for the contamination present on a sharp edge. Instead, here we define a corresponding edge contamination metric as the number of overhanging particles per meter of edge equal to and greater than the stated size. In this way, we can start to relate the particle distribution present on a surface to the particulate distribution found hanging over an edge. One important difference between surface and edge contamination is that particles present on the edge typically project some fraction of the total particle area over the edge. Only a portion of the particle is visible in projection, while the rest is hidden on top of or behind the edge.

Downloaded From: https://www.spiedigitallibrary.org/conference-proceedings-of-spie on 01 Nov 2023
Terms of Use: https://www.spiedigitallibrary.org/terms-of-use

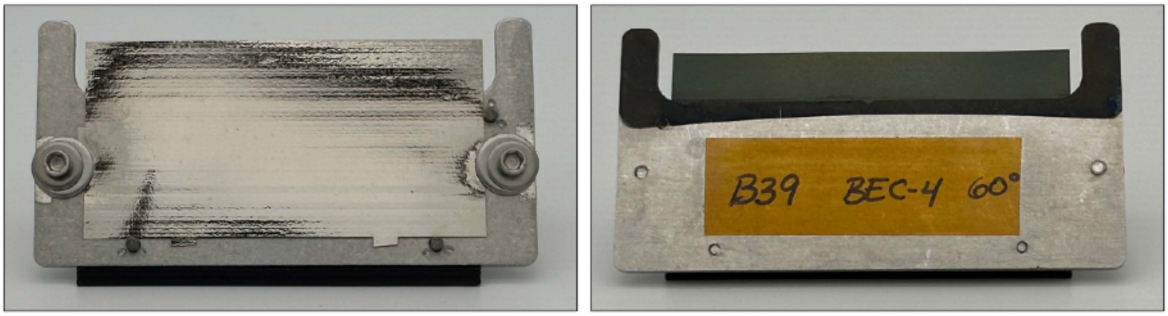
2. METHODOLOGY

2.1 Samples

2.1.1 AM Coupon Samples

Our samples consist of sharply-etched amorphous metal foils measuring 25x50 mm. The foil substrate is a Nickel-based brazing foil, MBF-30, manufactured by Metglas, Inc. as a 20-centimeter wide roll of foil measuring 38 µm in thickness. The foil is provided to an etching house, United Western Enterprises, where the coupons are patterned and etched to produce a sharp edge with a sub-micron radius of curvature. The majority of the samples under consideration are left uncoated, but a select number of coupons were coated with multi-layered anti-reflection coatings by ZeCoat Corporation.[7] Photos of both uncoated and coated sample coupons are shown in figure 2.

Except where noted, all AM sample foils were cleaned in an ultrasonic ethanol bath set to 50 °C for 30 minutes prior to contamination exposure. Once clean, each sample's surface and edge is characterized for particulate contamination, establishing a clean background measurement. Any particles found on the clean surface can later be subtracted from the contaminated surface, counting only the particles imparted during exposure. After characterization, the cleaned samples are transferred to a contamination chamber where they are exposed to contamination in the form of aerosolized test dust. Now dirty, the samples are again characterized for additional particulates on the surface and edge.



(a) (b)

Figure 2. (a) Uncoated AM coupon mounted in an aluminum sample holder showing the surface to be contaminated (b) Back-side of a coated coupon. The coating is applied only to one side, and is not visible from the front.

2.1.2 Calibration Mask

To serve as both a calibration for the experiment, and for model validation, three 5x5 inch sodalime glass masks were procured from Photo Sciences Inc. onto which ten submasks were deposited in chrome with a thickness of approximately 120 nm. When particulates settle onto the surface of the calibration mask, the chrome layer is thin enough in relation to the size of the particulates (microns to tens-of-microns in size), that it does not affect how the particle settles. Assuming that there are no electrostatic effects between the glass and the foil, the settling particle will have no preference towards or away from the submask edges.

To match the edge roughness of our etched AM samples, we have intentionally designed an edge roughness of ~15 µm into the submasks (see figure 3b). This detail ensures that the same image processing routine can be performed on the etched samples as well as on the calibration mask.

2.2 Contamination Chamber

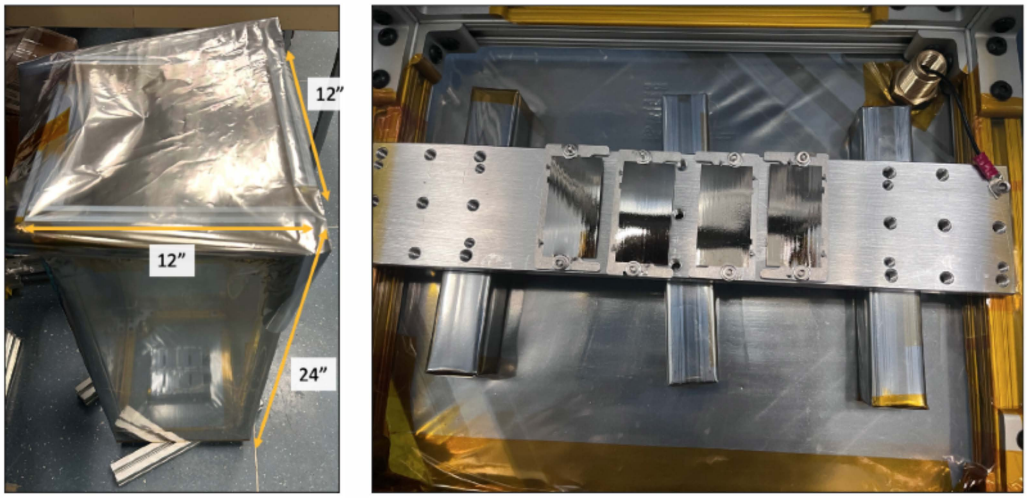
Our contamination chamber consists of a box frame constructed from 80/20 extruded aluminum wrapped in anti-static film with an access flap located at the top. An electrically grounded platform was placed on the floor of the contamination chamber onto which the AM samples were placed, ensuring that the samples have no net charge during exposure. The contamination chamber and the positioning of samples therein is represented in figure 4.

Downloaded From: https://www.spiedigitallibrary.org/conference-proceedings-of-spie on 01 Nov 2023
Terms of Use: https://www.spiedigitallibrary.org/terms-of-use



(a) (b)

Figure 3. (a) Picture of the 5x5 inch calibration mask showing the ten submasks arranged in a 5x2 grid pattern (b) Close up image of a submask corner detailing the roughly patterned edge.



(a) (b)

Figure 4. (a) Picture of the 80/20 box frame contamination chamber, wrapped in anti-static film. (b) Arrangement of AM samples on a grounded platform placed at the bottom of the contamination chamber.

2.3 Contaminants

We have chosen a generic silicate dust simulant, DUST-Y, available from Exolith Labs to disperse onto our samples. The bulk dust distribution has a mean particle size of 27.4 µm and a maximum particulate size of approximately 112 µm.[8]

2.4 Exposure

Prior to exposure, the inside surfaces of the contamination chamber, including the grounded platform, are wiped clean using an ethanol wipe to remove any dust or other debris that may already be present within the chamber. The samples are then transferred onto the grounded platform within the contamination chamber, and continuity with ground is checked with a multimeter.

Downloaded From: https://www.spiedigitallibrary.org/conference-proceedings-of-spie on 01 Nov 2023
Terms of Use: https://www.spiedigitallibrary.org/terms-of-use

A bulk amount of DUST-Y test dust is loaded into a fine mist powder sprayer, illustrated in figure 5a. Actuating the sprayer's bulb imparts a downward stream of air which impacts the bulk test dust, causing some dust to aerosolize within the sprayer. The increased air pressure directs the aerosolized dust to exit through the nozzle, producing a fine mist of effectively deagglomerated dust. The mist of dust is directed into the top of the chamber by slipping the nozzle of the sprayer underneath the anti-static film cover. The top cover of the contamination chamber ensures that the mist remains largely within the contamination chamber, and shields the chamber environment from outside air currents within the room. The sprayer is actuated a number of times within the chamber to produce a particular level of contamination. The angle and location of the sprayer are varied symmetrically in an attempt to produce uniform coverage. The aerosolized contamination is allowed to settle onto the samples over the course of 10-15 minutes. The mass of the sprayer is recorded before and after exposure, and we record the total mass of dust that entered the chamber. The amount of dust that settles onto the actual samples is a small, and unknown, fraction of this mass, but recording the total mass allows for some degree of repeatability between separate exposures. The goal is not to produce a known contamination level, but rather to produce uniform coverage across the samples in the chamber.



(a) (b)

Figure 5. (a) DUST-Y test dust within a fine mist powder sprayer. (b) Samples are exposed by actuating the bulb of the sprayer within the contamination chamber from the top. The dust is allowed to settle onto the samples over 10-15 minutes.

2.5 Characterization

2.5.1 MicroVu CMM

After exposure, the samples are individually transferred to a microVu Excel 1051UC for characterization.[9] The microVu is a coordinate measuring machine capable of performing repeated and automated measurements of parts up to about one meter in length. It can use several different magnifications, and has three different lighting capabilities. The head of the microVu is equipped with a programmable LED ring light that provides off-axis light from above. This feature illuminates the particles with minimal background reflection from the surface. A spotlight from below provides profile lighting, useful for silhouetting the edges of our samples, as seen in figure 6. The microVu is programmed to gather a set of images covering both the surface of the AM foil, as well as along the edge of the sample under consideration. These images are later processed to characterize the contamination present on the sample's surface and edge.

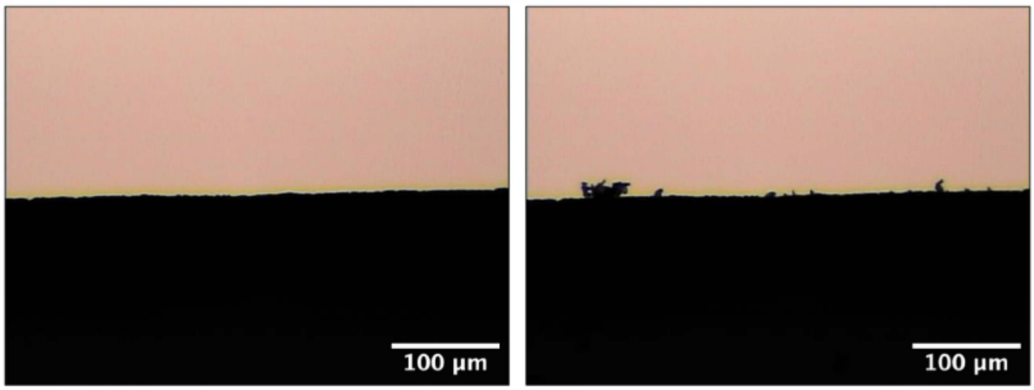
2.5.2 Surface Contamination

When imaging the sample's surface, the microVu is operated at a magnification of 170x, and the sample is illuminated from above using the LED ring light. The intensity of the lighting is balanced to avoid saturating the largest particulates, while attempting to adequately illuminate the smallest particulates.

The microVu gathers a 35x20 grid of images sampling a portion of the sample's AM surface. Adjacent frames are spaced such that 20% of the frame overlaps with its neighbor both horizontally and vertically. At a magnification of 170x, each individual frame spans a distance of 1.31x0.98 mm, and the entire grid is 36.9x15.9 mm for a total surveyed area of 586.5 mm^2 or 5.865×10^{-3} tenth square meters.

Downloaded From: https://www.spiedigitallibrary.org/conference-proceedings-of-spie on 01 Nov 2023
Terms of Use: https://www.spiedigitallibrary.org/terms-of-use

The grid of images is fed into an image processing routine implemented as an ImageJ[10] macro program that first stitches the grid of images together into a single large image containing all of the particles on the surface. This image is then thresholded, and the 'Analyze Particles' tool is used to count all the particles visible in the stitched image. For every particle detected, we record the particle's area, position, height, and width, and additionally, a summary describing the total number of particles detected, the average particle size, and the percent area coverage. Figure 7 illustrates the image processing routine which is first run on images gathered from the cleaned sample, and again after contamination. Any particles which are detected on the clean sample are later subtracted from the contaminated sample. The exported list of particles and their sizes is binned and scaled to form a cumulative particulate distribution. Finally, the PCL and slope of the contaminated surface can be calculated using a least squares fit to the cumulative particle distribution.



(a) (b)

Figure 6. (a) MicroVu image of a clean AM edge, exemplifying the roughness of the etched terminal edge. (b) Same region of edge imaged after contamination, showing the adhered edge particles.

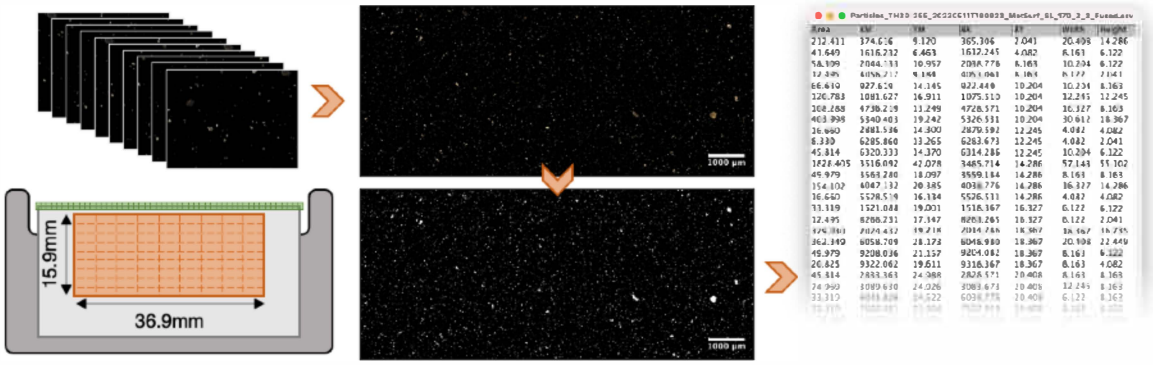


Figure 7. Illustration of the image processing routine for etched samples. A 35x20 grid of images (orange) is captured over the sample's surface, afterwards, 180 images (green) are captured in a row imaging the 50 mm of etched edge. Individual surface images are stitched together into one large image, which is then thresholded. Finally, the Analyze Particles tool identifies and characterizes each particle, exporting a list of sizes which is later binned into a particulate distribution.

All 10 submasks of the calibration mask are imaged in a similar fashion to the etched samples over the opaque regions and edges. In addition, to calibrate the different sensitivities of surface (170x) and profile (470x) lighting to particle sizes and reflectivities, clear areas of the mask are imaged twice under the two lighting and magnification conditions used for the surface and edge imaging. Figure 8 illustrates the regions of each submask that are imaged. The figure depicts only the top four submasks on the calibration mask. Orange areas in the figure indicate images taken at 170x magnification using surface lighting, while areas in green indicate images taken at 470x magnification and using profile lighting. First (1), a grid of images is taken covering the surface of

Downloaded From: https://www.spiedigitallibrary.org/conference-proceedings-of-spie on 01 Nov 2023
Terms of Use: https://www.spiedigitallibrary.org/terms-of-use

the metallic submask using the standard surface lighting condition at 170x magnification. Next (2, 3), two grids of images are taken covering regions of the glass above and below the submask using the same lighting condition. Afterwards (4, 5), the same regions above and below the submask are imaged using profile lighting at 470x, emulating the lighting conditions of the edge images. Each region, (2), (3), (4), and (5) cover approximately the same amount of surface area, Finally (6, 7), a series of images is taken covering the top and bottom edges of the submask, covering the entire 50 mm length of each edge.

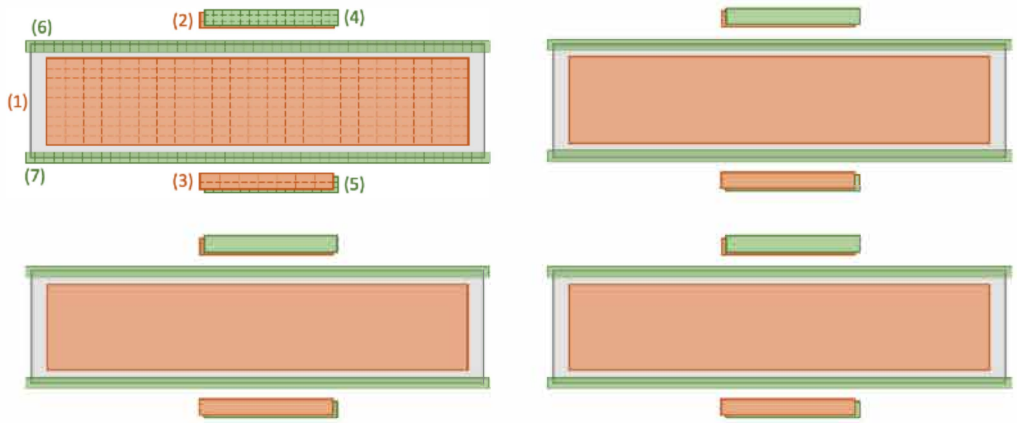


Figure 8. Imaging diagram showing the top four submasks on the calibration mask describing the different regions that are imaged. Green areas indicate images taken at 470x using profile lighting. Orange areas indicate images taken at 170x using surface lighting.

2.5.3 Edge Contamination

When imaging the sample's edge, the microVu is operated at a magnification of 470x using profile lighting producing a silhouette of the sample's edge. Here, the intensity of profile lighting was set to produce an adequate, non-saturating, level of background light. Just as for the surface, the edge of each sample is imaged after cleaning, and again after contamination. One change, however, is that rather than stitching the images together, here we treat each frame along the edge separately. The microVu gathers a total of 180 images covering the entire 50 mm length of the sample, with 40% of each frame overlapping the next. This spacing ensures that every particle is counted at least once, but also means that some particles may appear in two frames and get double-counted. These duplicate particles are later removed during post-processing.

Distinguishing individual edge particulates overhanging the edge of a sample requires knowledge of where the edge ends and the particle begins. This poses a challenge, as the etched edges of our samples have an edge roughness of approximately 15 µm, meaning the edge cannot be approximated by a straight line. Instead, a registration step is performed to align images of the clean edge to corresponding images of the contaminated edge. The descriptor-based registration routine in ImageJ identifies unique patterns in the rough edge visible in the two images, complicated by the fact that particulates are typically present in the contaminated image, obscuring parts of the edge. Indeed, if a sample contains too much contamination, this registration step fails, as the distinguishing features of the etched edge are increasingly covered by particulates.

Once aligned, the contaminated image is subtracted from the clean image leaving a largely black image where the two aligned images are identical. Where particles appear on the contaminated edge and obscure the background, the differenced image shows bright spots in the shape of the edge particulates. The differenced images can then be thresholded and analyzed for particles in much the same way as for the surface particulates. The processing routine generates a list of detected edge particles, and their projected areas, which is later binned into an edge particulate distribution. It is important to note that only the portion of the particle projecting out over the edge is detected. In that sense, the reported size of the edge particulates is the area which overhangs the edge, not the area of the full particulate, as is the case in the surface characterization.

Downloaded From: https://www.spiedigitallibrary.org/conference-proceedings-of-spie on 01 Nov 2023
Terms of Use: https://www.spiedigitallibrary.org/terms-of-use

2.5.4 Scatter Testing

The Single-Angle Scatterometer (SAS) at JPL, shown in figure 9, is an instrument developed to measure light scattered from starshade optical edges. The sample edge is held normal to a monochromatic source which illuminates the edge from below. Light scatters off of the edge, and a portion of that light is captured by a microscope objective held at a 30° angle above the plane of the edge. The captured light is imaged onto a camera where the light is integrated and calibrated against another scatterometer, the Multi-Angle Scatterometer at JPL, measuring the scatter from the edge at that location. The instrument then translates along the length of the edge, and takes another picture, measuring the scatter at this new location. In this way, the instrument starts at one end of the sample, and translates along its edge taking scatter measurements along the way at predefined intervals. The edge scatter can then be plotted as a function of position along the edge. The fractional scatter units presented here, e.g. figure 10, represent the fractional intensity of light scattered by the edge, averaged over the Sun angles 45°-75°, and integrated over edge orientations −90° - 90° (in the plane of the edge) at a distance of 1 m. These units correspond directly to those obtained by the two-dimensional Lumerical model described in McKeithen et. al.[7] The detailed instrument calibration process is described in Shaklan et. al.[4]

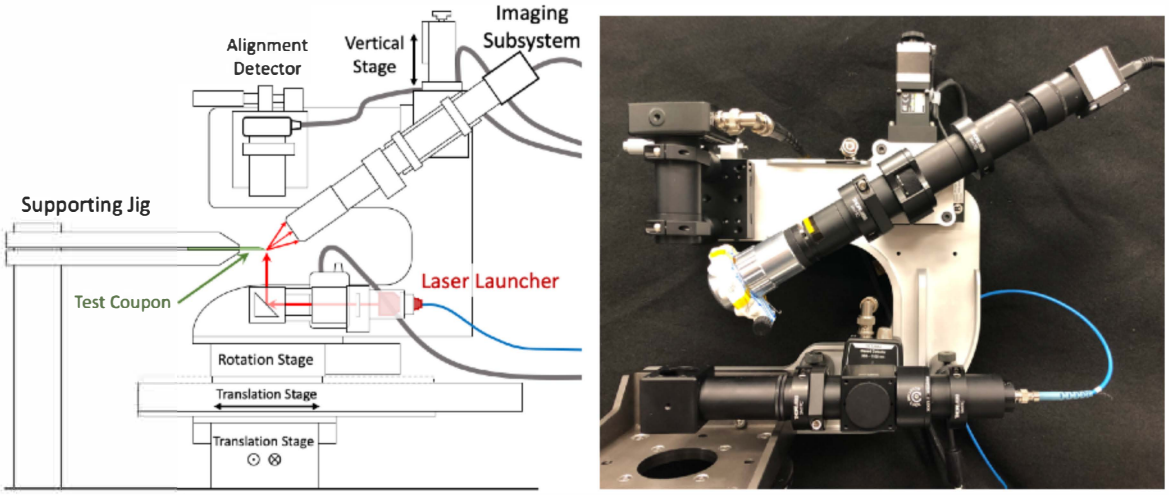


Figure 9. (a) Single-Angle Scatterometer (SAS) schematic. Monochromatic light strikes the sample from below which scatters light into the microscope objective. The instrument translates along the length of the edge (in and out of the plane of the paper) taking measurements of the scatter along the way. (b) Picture of the instrument showing the imaging system without a sample in place.

Here, each sample edge was measured in both a clean and contaminated state. An example plot from coated sample B33 is shown in figure 10, where a clear increase caused by the exposure to contamination is evident. Note that the baseline (clean) measurement is not completely uniform along the length of the sample, as seen in the region from 40-45 mm. This variability has many sources, from etching non-uniformities, to defects in the metal foil or in the coating, to handling damage. All of these must be minimized to maintain a sharp, uniform, and dim optical edge. However, the additional increase in scatter caused by contamination is independent of the initial (clean) scatter performance.

Differencing the contaminated and clean scatter measurements yields the net scatter increase due to the additional contamination. This net increase is later correlated with the detected contamination on the edge and the surface.

3. SURFACE-TO-EDGE MODEL

While we currently have the ability to directly measure the level of edge contamination present on a sample edge, this won't be possible over the course of the entire lifecycle of the starshade. The optical edges, unless

Downloaded From: https://www.spiedigitallibrary.org/conference-proceedings-of-spie on 01 Nov 2023
Terms of Use: https://www.spiedigitallibrary.org/terms-of-use

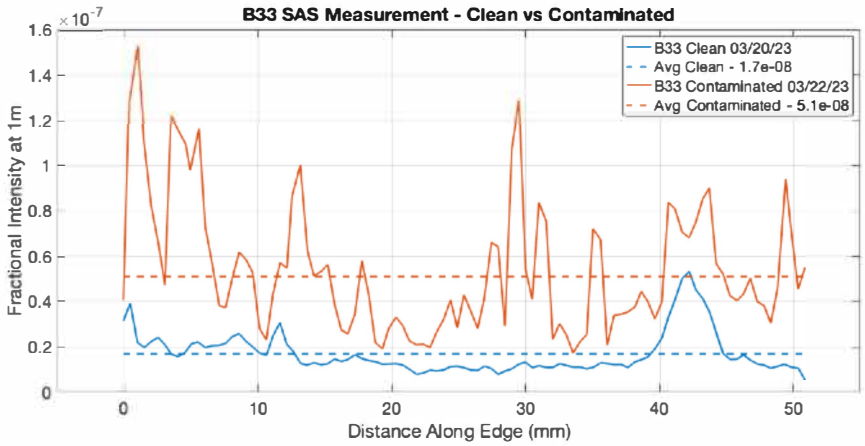


Figure 10. Single-Angle Scatterometer (SAS) measurements of a coated AM sample B33 taken before and after contamination. The difference between the orange and blue lines is the increased scatter due to the additional contamination on the edge of the sample. Data are presented with a roughly 1 mm linear resolution.

protected, will accumulate contamination throughout the manufacturing, assembly and testing processes, as well during stowage, launch, and even on-orbit, and it won't be possible to examine the edges in detail during much of this time. We must rely on silicon witness plate measurements to estimate the particulate contamination level present on the starshade's surface, then use this to predict the level of contamination expected on the edge, and finally correlate this to an increase in solar glint. Ultimately, we can then establish a contamination requirement that links surface contamination to an increase in edge glint.

With the goal to predict the level of edge contamination from a surface distribution, a simple model was developed which assumes that the presence of an edge would have no effect on the distribution of particulates on a surface. In essence, we ask, given a distribution of particulates on a surface, if a line is drawn through the surface at random, how many particles should we expect the line to intersect?

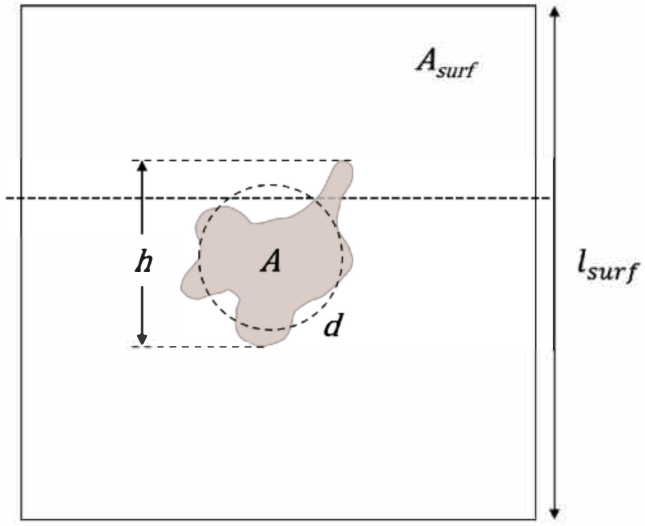


Figure 11.

Consider a single particle of area, A, located on a surface with area A_{surf} and side lengths $l_{\text{surf}} = \sqrt{A_{\text{surf}}}$. The bounding height of the particle, h, is the furthest extent of the particle in the vertical direction. The circular

Downloaded From: https://www.spiedigitallibrary.org/conference-proceedings-of-spie on 01 Nov 2023
Terms of Use: https://www.spiedigitallibrary.org/terms-of-use

diameter, d, is the diameter of the circle having the same area as the particle, $d = \sqrt{\frac{4}{\pi} * A}$.

If a horizontal line is drawn at random through the surface, simulating the presence of an 'edge', the probability of intersecting the particle, P, is the ratio of the height of the particle to the height of the surface.

$$P = \frac{h}{l_{\text{surf}}} \tag{3}$$

If the surface contains $N_{\text{surf}}(A)$ total particles with area A, then the number of particulates per unit area is given by $n_{\text{surf}} = N_{\text{surf}}/A_{\text{surf}}$. Then, assuming that these particulates are uniformly distributed over A_{surf}, the number of particles intersecting the random edge, as a function of particle area, A, is given by

$$N_{\text{edge}}(A) = N_{\text{surf}}(A) * \overline{P}(A) = N_{\text{surf}}(A) * \frac{\overline{h}(A)}{l_{\text{surf}}} \tag{4}$$

Where $\overline{P}(A) = \overline{h}(A)/l_{\text{surf}}$ is the average probability of intersecting a particle of area A, and $\overline{h}(A)$ is the average height of those particles with area A:

$$\overline{h}(A) = \frac{1}{N_{\text{surf}}(A)} * \sum_{i=1}^{N_{\text{surf}}(A)} h_i(A) \tag{5}$$

The expected number of particulates intersecting the edge per unit length is then

$$n_{\text{edge}}(A) = \frac{N_{\text{edge}}(A)}{l_{\text{surf}}} = \frac{N_{\text{surf}}(A) * \overline{h}(A)}{l_{\text{surf}}^2} = \overline{h}(A) * \frac{N_{\text{surf}}(A)}{A_{\text{surf}}} = \overline{h}(A) * n_{\text{surf}}(A) \tag{6}$$

For the irregularly shaped particulates present in this study, the average particle height, $\overline{h}(A)$, is typically larger than the particle's circular diameter, $d(A)$. The measured ratio $\overline{h}(A)/d(A)$ is shown in figure 12 for particles of varying areas. This ratio tends towards one for the smallest particles, indicating that the particulates appear more circular at these small sizes. At larger sizes, the irregularity of the particulates becomes more apparent, as the average height of the particle grows to nearly 20% higher than its circular diameter. The shape of this ratio is specific to the DUST-Y test dust, and different dust simulants will produce different curves. In the present results, the average height of the particles within a given bin is calculated from equation 5 and used to calculate $n_{edge}(A)$ in equation 6. This method becomes less reliable at the largest particle sizes where the number of particles present on the surface decreases.

Equation 6 describes the distribution of particles expected to intersect a randomly drawn 'edge', as a function of particle area. This quantity is not directly measured, however, as only the portion of the particulate projecting out over the edge is visible to the camera. The measured edge particulate distribution presented here is binned according to the area of the particle overhanging the edge.

We use the predicted distribution to estimate the total amount of particulate area which we expect to overhang the edge from the surface contamination. We assume that, on average, half of the particle's area will overhang the edge. Summing the product of the number of particles with the overhanging area corresponding to each bin yields the total particulate area which overhangs the edge.

$$A_{\text{edge, total}} = \sum_{i=1}^{\infty} N_{\text{edge}}(A)_i * \frac{A_i}{2} \tag{7}$$

In practice, we have oversimplified the edge prediction by computing only the average number of overlapping edge particles as a function of the distribution of particle areas on the surface. A more accurate calculation would consider the range of overlap areas and convolve the edge distribution with particle shape. For example,

Downloaded From: https://www.spiedigitallibrary.org/conference-proceedings-of-spie on 01 Nov 2023
Terms of Use: https://www.spiedigitallibrary.org/terms-of-use

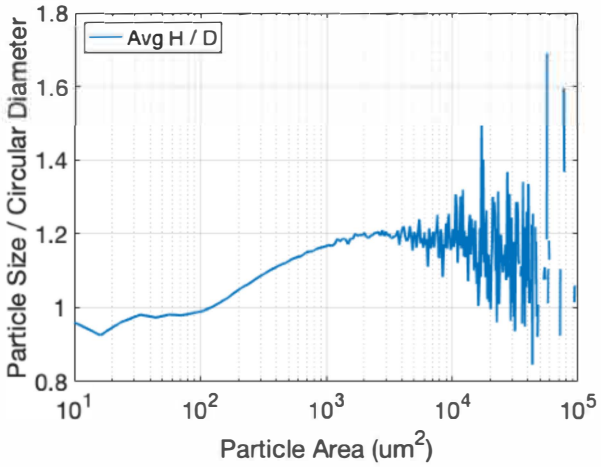


Figure 12. Ratio of the particle's average height to its circular diameter for particles of varying sizes. The ratio tends towards one at small particle sizes, and approaches ~ 1.2 for larger particles.

for perfectly circular particles, this spread is equivalent to the convolution of a circle with the Heaviside step function. However, this function is unknown for the range of irregular particles used here.

To account for this simplification, we employ an additional term to the edge prediction model that scales with square root of particle diameter. We found with this scaling law, eq. 7 accurately predicts the measured edge data for the calibration mask.

4. EXPERIMENTAL RESULTS

4.1 Calibration Mask

The calibration masks, being too delicate to subject to sonication, were cleaned by rinsing with an excess of ethanol, and were air dried before being characterized by the microVu imaging routine. Afterwards, the clean masks were transferred into the contamination chamber, where each mask was exposed separately to different amounts of DUST-Y contamination ($\sim$30 mg and $\sim$20 mg respectively). After allowing the dust to settle for $\sim$ 10 minutes, the now contaminated masks were transferred back to the microVu for the second round of characterization.

4.1.1 Imaging Calibration

First, we examine the regions of the mask which were imaged under the two lighting conditions above and below each submask, comparing regions (2) and (3) from figure 8 to (4) and (5). Figure 13 presents the total number of particulates found on the surface for both calibration mask exposures. The particulates from each of the 40 total regions across the two exposures have been totaled to form a combined surface particulate distribution where the list of particles returned from the image processing routine have been binned according to the particle's area. The blue line displays the number of surface particulates found by imaging the calibration mask at the high magnification 470x and using profile lighting. The orange line displays the number of surface particulates found by imaging the same regions of the calibration mask at a lower magnification, 170x and using LED lighting from above. The ratio of these curves (figure 13b) serves as the calibration between the two lighting conditions. Where the plotted ratio becomes noisy due to low particulate counts, the imaging calibration is smoothed such that it approaches a value of one as particulate size increases and the difference between the two lighting conditions becomes negligible.

Downloaded From: https://www.spiedigitallibrary.org/conference-proceedings-of-spie on 01 Nov 2023
Terms of Use: https://www.spiedigitallibrary.org/terms-of-use

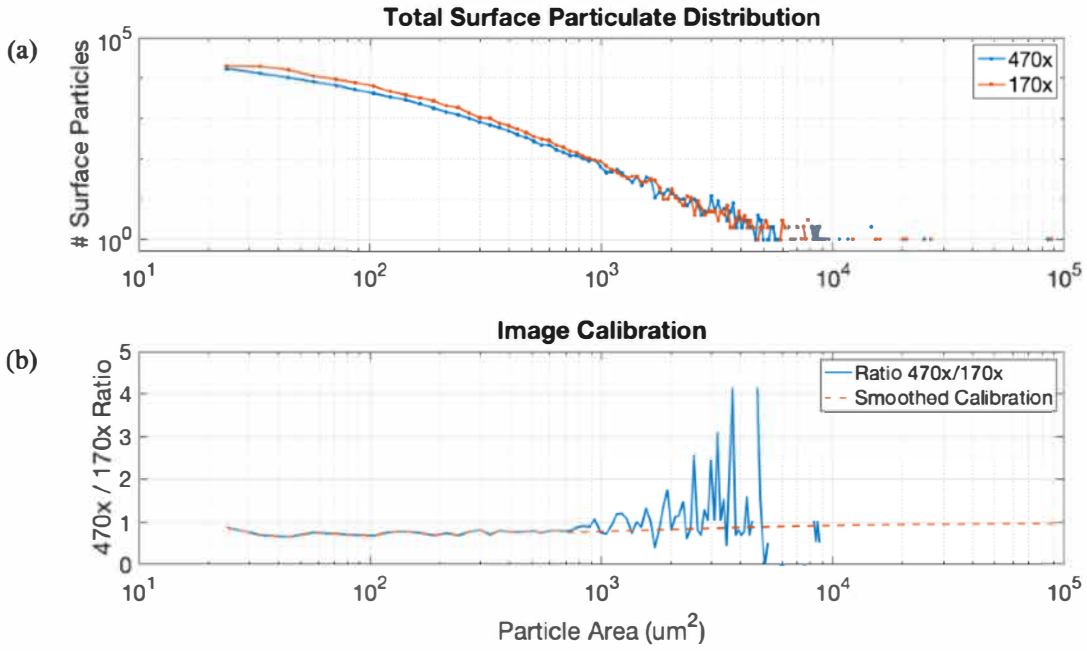


Figure 13. (a) Total surface particulate distributions measured using different magnifications and lighting conditions. The same region of the calibration mask measured once at 170x with LED lighting, and once at 470x with profile lighting to emulate the conditions used to image the surface and edge, respectively, of the etched samples. (b) Ratio of the two particulate distributions, which is smoothed where the data becomes noisy, to be applied as an imaging calibration between surface and edge images.

4.1.2 Model Validation

Now, we compare the surface particulate distribution measured from region (1) in figure 8 to the combined edge particulate distribution measured from (6) and (7) and attempt to relate the two using the surface-to-edge model. Figure 14 shows the total surface (a) and edge (b) particulate distributions measured from the two combined exposures, totalling all ten submasks. For clarity, here we display the distributions as a raw count, the actual number of particulates which were detected across the two calibration mask exposures. It is sometimes useful, however, to standardize the surface distribution as the number of particulates per tenth square meter, particularly in order to classify the distribution with a PCL and slope using IEST-STD-CC1246E.

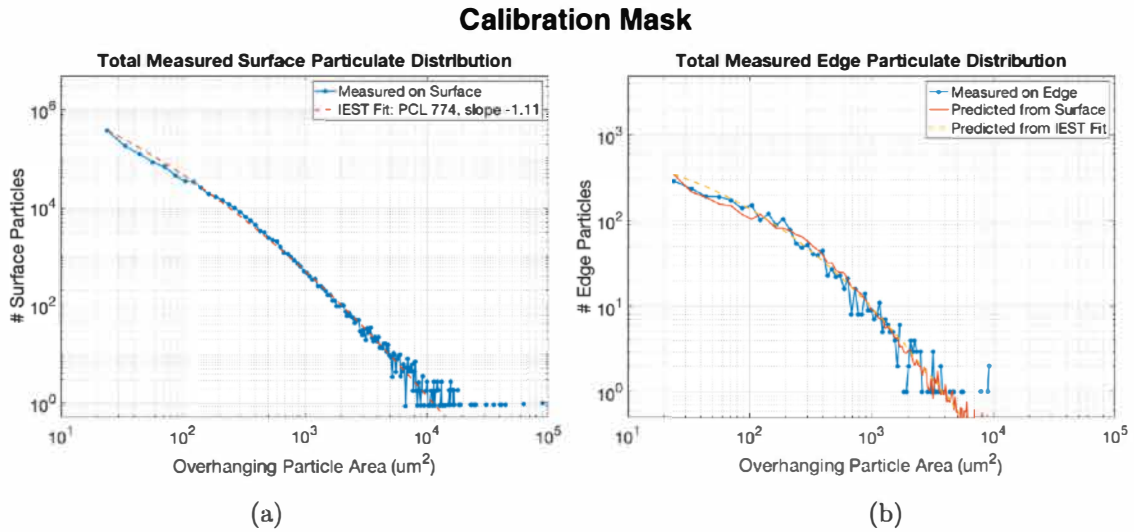
Figure 14(a) presents the total surface particulate distribution measured from the two combined exposures. A total of 9077.2 mm^2 of surface was imaged to form this combined distribution. This distribution is scaled to the basis of tenth square meters and is fitted to an IEST distribution using a least-squares fit in $\log - \log^2$ space. The total surface particulate distribution exhibits a PCL of 774 with a slope of -1.10.

Using equation 6, we calculate $N_{\mathbf{edge}}(A)$ from the total surface distribution as well as from the fitted IEST distribution, apply the square root of diameter modification to account for the spread of overhanging areas, and compare to the total number of edge particles measured along 2000 mm total length of edge. As seen in figure 14(b), the number of particulates predicted from the surface distribution and IEST fit closely matches the measured number of edge particles, indicating that the surface-to-edge model works well. On the calibration mask where the glass substrate prevents particulates from falling off of the edge, the number of particulates detected overhanging the edge matches the number of particulates that intersect a line drawn randomly through the contaminated surface.

4.2 Etched Samples

A total of four unique contamination exposures were performed over the course of the experiment. For each exposure, a number of samples ranging from four to eight were placed within the contamination chamber, where

Downloaded From: https://www.spiedigitallibrary.org/conference-proceedings-of-spie on 01 Nov 2023
Terms of Use: https://www.spiedigitallibrary.org/terms-of-use



(a) (b)

Figure 14. (a) Total surface particulate distribution detected on the calibration mask is shown in blue. The orange line is the IEST distribution with the given PCL and slope, which has been fit to the surface distribution. (b) Total edge particulate distribution detected on the calibration mask is shown in blue. Compared to that, is the prediction generated from the surface and from the IEST fit, which both show good agreement across a range of particle sizes.

a measured mass of DUST-Y test dust was aerosolized and allowed to settle onto the samples. A total of 22 samples were characterized while both clean and contaminated. The edge and surface images were processed following exactly the same protocol as the calibration mask images. The amount of DUST-Y test dust introduced into the chamber in each exposure was intentionally varied, from a minimum of 12 mg to a maximum of 53 mg in order to attain varying contamination levels across the samples. The samples exposed at the same time generally received a similar level of contamination to their neighbors. Consistency, however, is not necessarily the goal. Rather, the goal is to correlate whatever amount landed on the surface of a particular sample to that which overhangs the edge. The samples tested included six that were coated with a thin anti-reflection coating, similar to that shown in figure 2. The level of contamination achieved on these coated samples was not found to differ significantly from that of the uncoated samples.

Figure 15(a) shows the total combined surface particulate distributions measured on the 22 samples, from a total surface area of 12 908 mm^2. Fitting to the IEST distribution results in a distribution with a PCL of 909 and a slope of -1.10.

Just as for the calibration mask, the surface-to-edge model is employed to predict the distribution of edge particles. Figure 15b compares that prediction to the number of edge particulates measured over 1100 mm of edge across the 22 samples. We find that the surface and IEST fit are inadequate to predict the distribution of edge particulates. For particles less than ~200 μm^2, we find more particulates than expected from the surface, while above 200 μm^2, we find fewer particulates than expected.

When particulates settle near the edge of the calibration mask, they more or less settle where they land and are not influenced by the thin chrome edge. In contrast, when particulates settle near the edge of the etched samples, there is a non-zero chance that the particulates fall off of the edge, depending on the position of the particulate relative to the edge, the particulate's shape, weight, velocity, and many other factors. The excess particulates that we observe at small particulate sizes additionally suggests the presence of complex adhesion forces which may cause small particulates to adhere to the edge more readily than on the calibration mask. The dearth of large particles may be due to gravity acting on those that are teetering with their center of mass beyond the edge.

Figure 16(a) compares the two edge particulate distributions obtained using the calibration mask and the 22 etched samples, where each distribution is normalized by the total number of particulates, such that the y-axis describes the proportion of the total particulates that fall into each particulate bin. The calibration mask

Downloaded From: https://www.spiedigitallibrary.org/conference-proceedings-of-spie on 01 Nov 2023
Terms of Use: https://www.spiedigitallibrary.org/terms-of-use

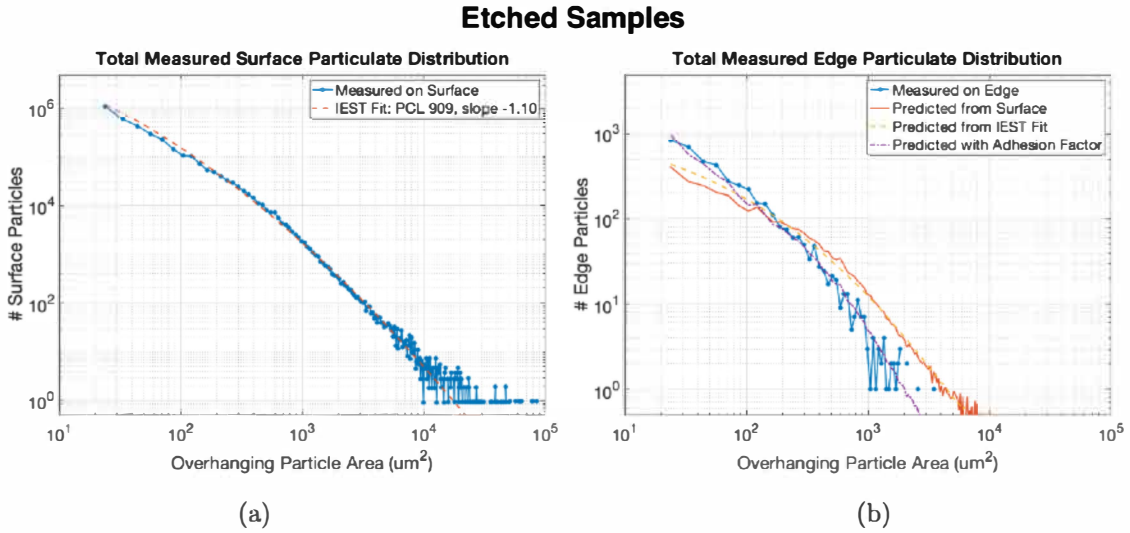


Figure 15. (a) Total surface particulate distribution detected on the etched samples, and a fit to the IEST distribution. (b) Total edge particulate distribution detected on the etched samples, compared to predictions from the surface.

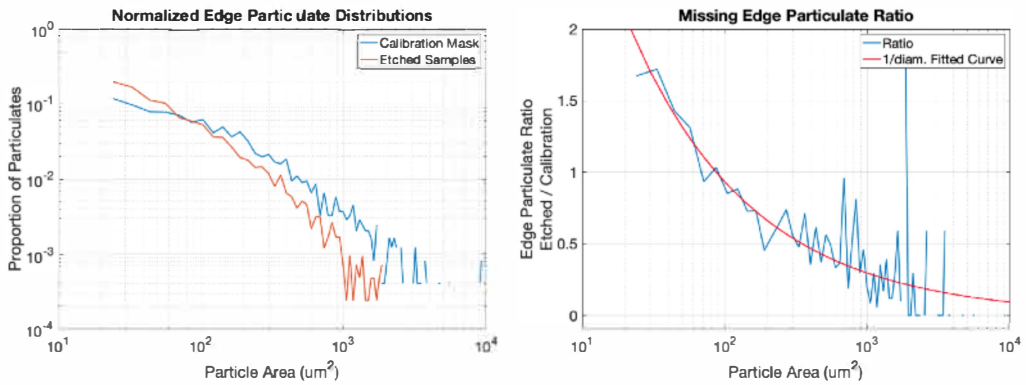
and the etched samples were each exposed to differing amounts of contamination, but the same test dust and exposure method was used, so while the overall amount of contamination differs, the *distribution* of particulates isn't expected to change between the two experiments. By normalizing each distribution to the total number of particulates, we find that particles larger than $\sim 100\,\mu m^2$ on the etched samples adhere to the edge to a lesser degree than on the calibration mask. Conversely, particles less than $\sim 100\,\mu m^2$ seem to adhere to the etched edge even more strongly than on the calibration mask. The ratio of these two curves represents what we are calling the 'adhesion' factor. This ratio, plotted in figure 16(b), describes the probability that a particulate of a given size will adhere to the edge. A lower probability results in fewer particulates of that size adhering to the edge. We find that this adhesion factor ratio decreases proportionally to the inverse of the particle diameter. That is, the larger the particulate is, the less likely it is to adhere, and the more likely it is to fall off, in proportion to the diameter of the particle. We apply this adhesion factor to the surface prediction to account for the difference between the calibration mask and the etched samples (purple curve in figure 15(b). With this additional term, we find good agreement with the measured edge particulate distribution.

4.2.1 Scatter Results

Each of the 22 etched samples were scatter tested on the SAS before and after contamination. The average scatter level after contamination is subtracted from the average scatter level from before contamination, yielding a net scatter increase for that sample. After the samples are imaged, the area of all edge particulates detected is summed, giving us the total overhanging edge particulate area present on that sample. Figure 18 shows a clear, positive relationship between edge particulate area and increased scatter for the 22 measured samples. The slope of the linear fit describes the amount of increased scatter per square micron of edge contamination.

To predict the increase in scatter from the contaminated surface, we first compute the edge distribution from the surface distribution, including the adhesion factor. We then integrate the edge distribution to predict the total edge particulate area we expect to find on the edge of the sample. Finally, the slope from figure 18 is used to convert from the total edge particulate area, to a prediction of the resulting scatter increase. We compare the scatter increase predictions to measurements in figure 18. The first column describes the total increase in scatter measured from the 22 samples. The second column is a scatter prediction made using the direct measurement of the edge particulate area and the slope of the linear fit from above. The third and fourth columns are the scatter predictions from the surface distribution and IEST fit, which both exhibit a gross over-prediction. Finally, the fourth column shows the scatter prediction made after incorporating the adhesion factor. With the inclusion of the adhesion factor, the increase in scatter is predicted to within 3%.

Downloaded From: https://www.spiedigitallibrary.org/conference-proceedings-of-spie on 01 Nov 2023
Terms of Use: https://www.spiedigitallibrary.org/terms-of-use



(a) (b)

Figure 16. (a) Normalized edge particulate distributions for the calibration mask and the etched samples. Each distribution has been normalized based on the total number of edge particulates. (b) Ratio of the normalized edge distributions, representing the portion of particulates missing from the etched samples. The ratio decreases with particulate size inversely proportional to the particle diameter.

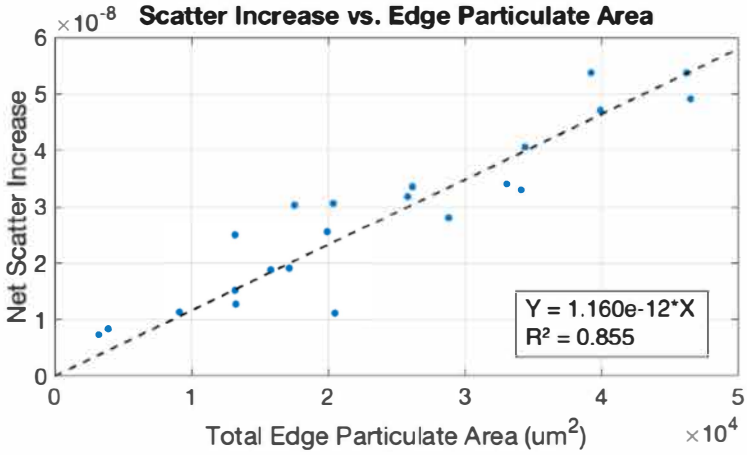


Figure 17. Relationship between the total edge particulate area and the corresponding scatter increase, showing a positive relationship. A linear fit finds that the slope of the distribution is $1.160 \times 10^{-12}\ \mu m^{-2}$

5. DISCUSSION

With the ability to accurately predict the level of edge scatter from a measured surface particulate contamination distribution, we turn our attention toward defining an on-orbit contamination requirement. Table 1 provides the mission parameters for three starshade concept missions: the Habitable Exoplanet Observatory (HabEx), and two concepts designed for the Habitable Worlds Observatory, a 35-m and a 60-m starshade.

Column 5 of Table 1, reproduced from Shaklan et. al.,[4] reports the visual magnitude of the mean brightness of the HabEx starshade, using uncoated optical edges, accounting for measurement uncertainty, and calculated at the IWA for a Sun angle of 65° which roughly corresponds to the scattering angle captured by the SAS. This defines the current requirement for uncoated optical edges, and corresponds to an instrument scatter value of 7.615×10^{-8}. McKeithen et. al.,[7] finds a 3.1 magnitude improvement when an optimized AR coating is applied to the optical edges. This improvement is captured in column 6 of Table 1, reporting the visual magnitude of the starshade with coated edges. The corresponding magnitudes for the two HWO starshades are obtained by geometrically scaling the HabEx magnitude according to the new mission's diameter and range. The brightness of the starshade scales proportionally to its diameter, and inversely proportional to the square of its range. For

Downloaded From: https://www.spiedigitallibrary.org/conference-proceedings-of-spie on 01 Nov 2023
Terms of Use: https://www.spiedigitallibrary.org/terms-of-use

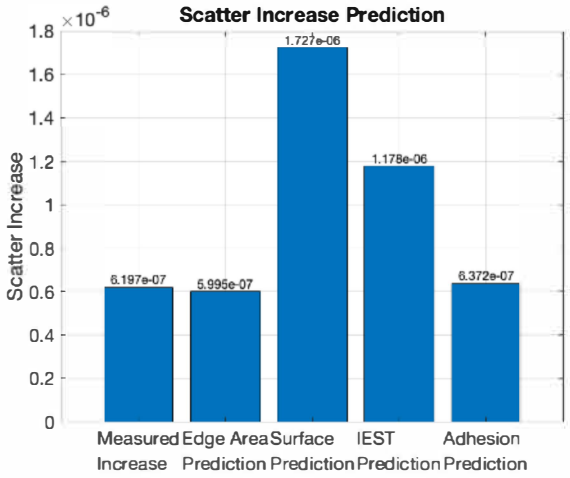


Figure 18. Scatter increase predictions compared to what we actually measured. The first column on the left describes the total increase in scatter from the 22 samples. The second column is the result obtained by using the measured edge particulate area. The third and fourth columns are the scatter predictions from the surface distribution and IEST fit. Finally, the fourth column shows the scatter prediction made after incorporating the adhesion factor.

Concept Mission	Diameter (m)	Range (Mm)	Bandpass (nm)	IWA Phot. 95% Conf. @ 65° (uncoated)	IWA Phot. 95% Conf. @ 65° (coated)
HabEx	52	76.0	300-1000	28.2	31.3
HWO-35m	35	55.5	250-500	27.9	31.0
HWO-60m	60	95.2	500-1000	28.5	31.6

Table 1. Mission parameters for the HabEx and Habitable Worlds Observatory (HWO) starshades. The last column represents the visual magnitude brightness of the starshade glint lobes using coated edges.

the HWO-35m starshade, the change in brightness, expressed as a difference in stellar magnitude can be found as:

$$-2.5 * \log_{10}(\frac{35}{52} * (\frac{55.5}{76.0})^{2}) = -0.3 \tag{8}$$

We apply a similar calculation for the 60-meter concept and report the uncontaminated edge glint brightness in Table 1.

To keep the level of edge contamination low enough that it doesn't significantly interfere with observations, it is desirable to keep this contribution dimmer than magnitude 33. For the HWO-35m starshade, this requires that the scatter due to contamination must appear to be $33.0-27.9 = 5.1$ visual magnitudes fainter than the uncoated edges. This corresponds to a target instrument scatter value of $10^{-5.1/2.5} * 7.615 \times 10^{-8} = 0.9\% * 7.615 \times 10^{-8} = 6.945 \times 10^{-10}$. For the HWO-60m concept, a similar calculation finds that an instrument scatter value of 1.207×10^{-9} corresponds to a visual magnitude of 33 for the contamination component.

At this point, the question becomes, at what surface contamination level can we expect this level of scatter? When classifying a surface particulate distribution with a product cleanliness level, it is important to consider the slope of the particulate distribution. For the same PCL, different slopes affect the relative proportion of large particulates to small, which, when combined with the surface-to-edge model, result in significantly different scatter predictions.

The standard slope of -0.926 used in equation 1 is meant to represent the distribution of particulates on a surface which has just been cleaned. The distribution of particulates on the etched samples presented above exhibit a steeper slope of -1.1, though this is largely a result of our dispersal method, and the bulk particulate

Downloaded From: https://www.spiedigitallibrary.org/conference-proceedings-of-spie on 01 Nov 2023
Terms of Use: https://www.spiedigitallibrary.org/terms-of-use

distribution present in the DUST-Y simulant, and we do not expect this distribution to be representative of actual particle fallout. According to the IEST-STD-CC1246E document, actual environmental fallout follows the same distribution as in equation 1, but with a much lower slope ranging between -0.3 and -0.5, and specifies that a slope of -0.4 shall be used to assign a limit on particle fallout. The final surface distribution will be some combination of the cleaned distribution with fallout from the spacecraft integration process, and may include additional contributions from particulate distribution while venting during launch vehicle ascent.

Using the standard slope of -0.926, we simulate surface particle distributions from a range of cleanliness levels. We then feed these surface distributions through the surface-to-edge model to simulate the distribution of particles that we expect to find on the edge, accounting for the likelihood that particles will adhere to the edge. From the predicted edge particle distribution, the projected surface area of the edge particulates is totaled, which is then converted into a scatter prediction based on the relationship found in figure 18. The resulting scatter prediction due to contamination can then be converted into an on-sky visual magnitude for both HWO starshade concepts. Figure 19 shows the resulting scatter and magnitude predictions for the two starshade concepts as a function of product cleanliness level. The blue line shows the predicted instrument scatter value, and the orange dashed lines plot the on-sky magnitude for the two starshades. For the two starshades, we find that PCL 410 for the 35-meter, and PCL 460 for the 60-meter starshade is sufficient to limit the resulting on-sky magnitude to 33.

Using equation 2, we estimate that these PCL values correspond to a surface PAC of 0.11% and 0.19% for the 35-meter, and 60-meter starshades respectively.

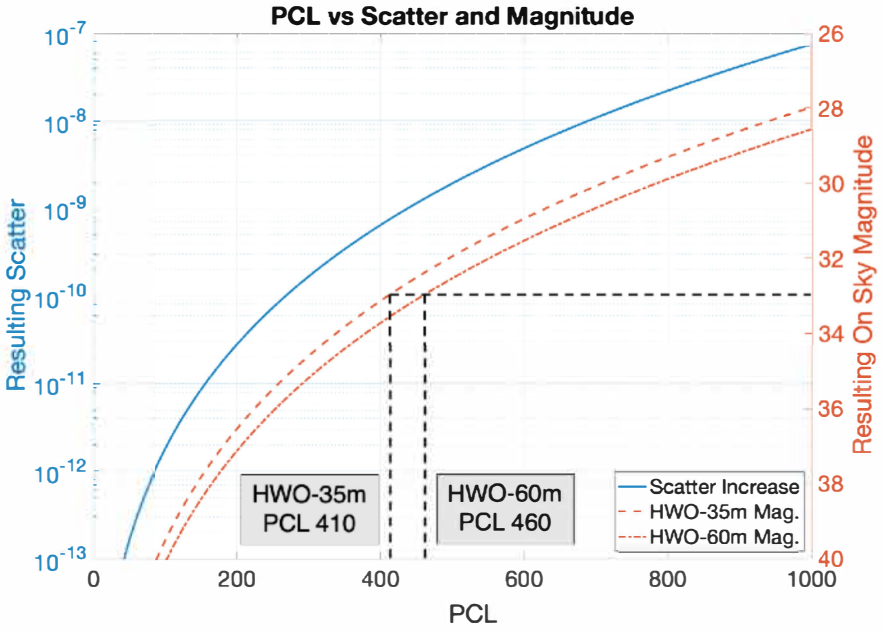


Figure 19. Predicted scatter increase and resulting on-sky magnitude for the HWO starshade concepts, plotted as a function of product cleanliness level. PCL 410 for the 35-meter, and PCL 460 for the 60-meter starshade limits the on-sky brightness to magnitude 33.

6. CONCLUSION

We have developed a simple model to predict the level of edge contamination from the surface which assumes that the edge contamination is equivalent to drawing a line through the contaminated surface. We have validated this model using a glass calibration mask where the glass substrate prevents particulates from falling off of the edge.

Downloaded From: https://www.spiedigitallibrary.org/conference-proceedings-of-spie on 01 Nov 2023
Terms of Use: https://www.spiedigitallibrary.org/terms-of-use

By comparing the edge contamination between the calibration mask and the etched samples, we find that, after accounting for the nominal size distribution, edge particulates appear with a frequency that is inversely proportional to their diameter. After incorporating this effect, our model is able to accurately predict the level of edge contamination from a characterization of the surface. We have correlated the level of edge contamination to an increase in scattered light, and have used this relationship to determine that PAC levels of 0.1 percent and 0.2 percent are required for the HWO-35m and HWO-60m concepts, respectively. These requirements assume a 'clean' surface with a slope of -0.926. While this is appropriate for surfaces that have been wiped clean, in reality the starshade will be subject to fallout that will add to the contamination level. The additional scatter from the fallout requires further analysis.

This research was carried out at the Jet Propulsion Laboratory, California Institute of Technology, under a contract with the National Aeronautics and Space Administration (80NM0018D0004).

©2023. All rights reserved.

REFERENCES

[1] National Academies of Sciences, E. and Medicine, [*Pathways to Discovery in Astronomy and Astrophysics for the 2020s*], The National Academies Press, Washington, DC (2021).

[2] Arenberg, J. W., Harness, A. D., and Jensen-Clem, R. M., "Special Section on Starshades: Overview and a Dialogue," *Journal of Astronomical Telescopes, Instruments, and Systems* **7**(2), 021201 (2021).

[3] Shaklan, S., Marchen, L., Cady, E., et al., "Error budgets for the Exoplanet Starshade (Exo-S) probe-class mission study," in [*Techniques and Instrumentation for Detection of Exoplanets VII*], *Proc. SPIE* **9605**, 314 327 (Aug. 2015). [doi:10.1117/12.2190384].

[4] Shaklan, S., Hilgemann, E., McKeithen, D., Martin, S. R., Steeves, J., Webb, D., and Lisman, D., "Solar glint from uncoated starshade optical edges," *Journal of Astronomical Telescopes, Instruments, and Systems* **7** (Jan 2021).

[5] Institute of Environmental Sciences and Technology, *IEST-STD-CC1246E: Contamination Control Division Standard 1246E* (Feb. 2013).

[6] Ma, P. T., Fong, M. C., and Lee, A. L., "Surface particle obscuration and brdf predictions," *Scatter from Optical Components* (Jan 1990).

[7] McKeithen, D., Shaklan, S., Sheikh, D., Balasubramanian, K., and Lowe, E., "Antireflection coatings on starshade optical edges for solar glint suppression," *Journal of Astronomical Telescopes, Instruments, and Systems* **7** (Jan 2021).

[8] Exolith Lab, *DUST-Y Silicate Dust Simulant Fact Sheet* (2023).

[9] Micro-Vu, *Micro-Vu Excel Overview* (2023).

[10] Rasband, W., "Imagej." https://imagej.net/ij/ (1997 2023). Accessed: 2022-06-01.

Downloaded From: https://www.spiedigitallibrary.org/conference-proceedings-of-spie on 01 Nov 2023
Terms of Use: https://www.spiedigitallibrary.org/terms-of-use